

LA-SUB--96-52

RECEIVED

APR 12 1996

OSTI

APPLICATION OF MACH2 TO EXPLOSIVE MAGNETIC FLUX COMPRESSION GENERATORS

Improvements in Detonation Modeling

CONSULTANTS -

FINAL REPORT

6 APR 95 9:14

John J. Watrous and Michael H. Frese
April 27, 1994
Report 94-04

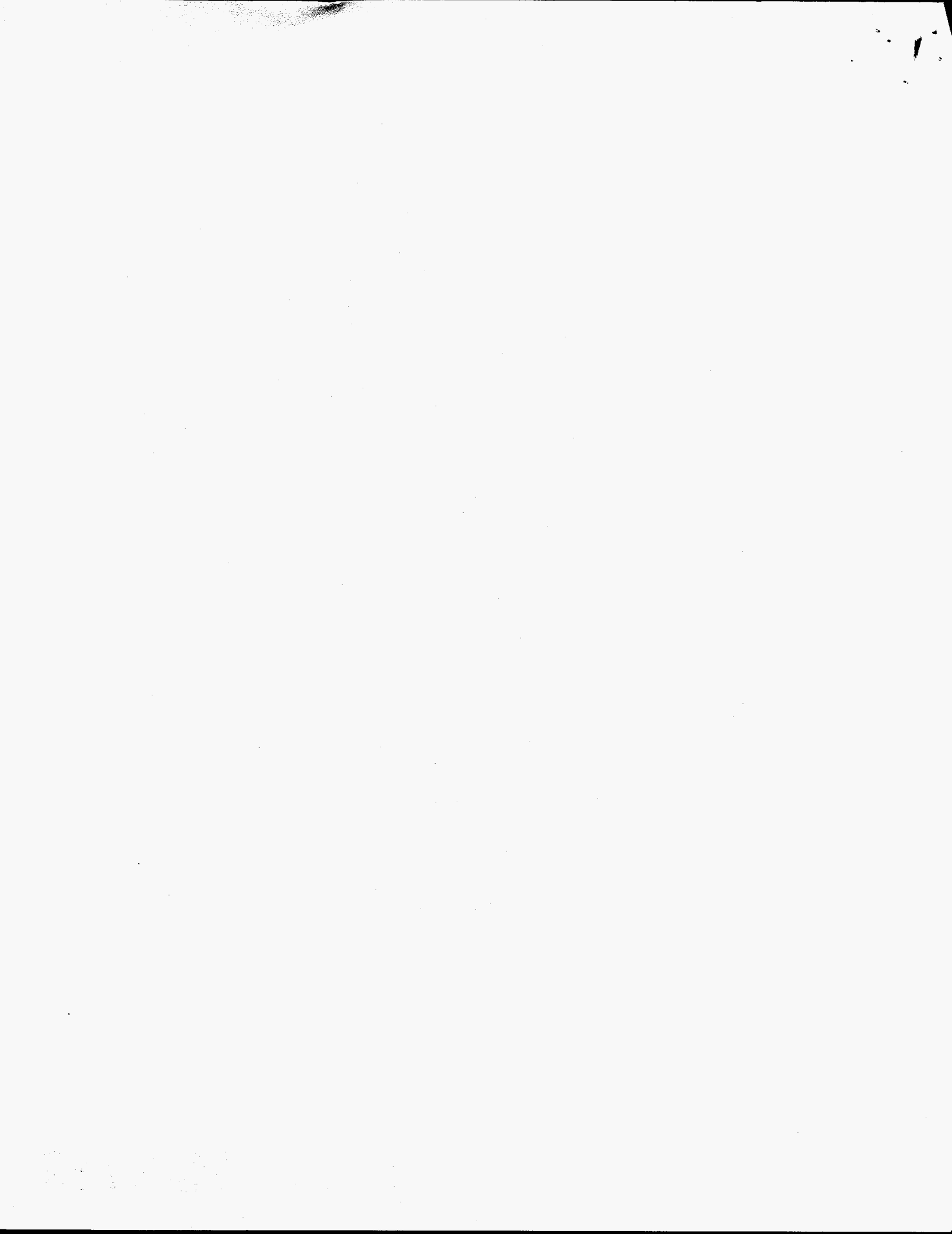
Los Alamos National Laboratory
Contract Number 768K0013-9H

DISCLAIMER

This report was prepared as an account of work sponsored by an agency of the United States Government. Neither the United States Government nor any agency thereof, nor any of their employees, makes any warranty, express or implied, or assumes any legal liability or responsibility for the accuracy, completeness, or usefulness of any information, apparatus, product, or process disclosed, or represents that its use would not infringe privately owned rights. Reference herein to any specific commercial product, process, or service by trade name, trademark, manufacturer, or otherwise does not necessarily constitute or imply its endorsement, recommendation, or favoring by the United States Government or any agency thereof. The views and opinions of authors expressed herein do not necessarily state or reflect those of the United States Government or any agency thereof.

DISTRIBUTION OF THIS DOCUMENT IS UNLIMITED

MASTER



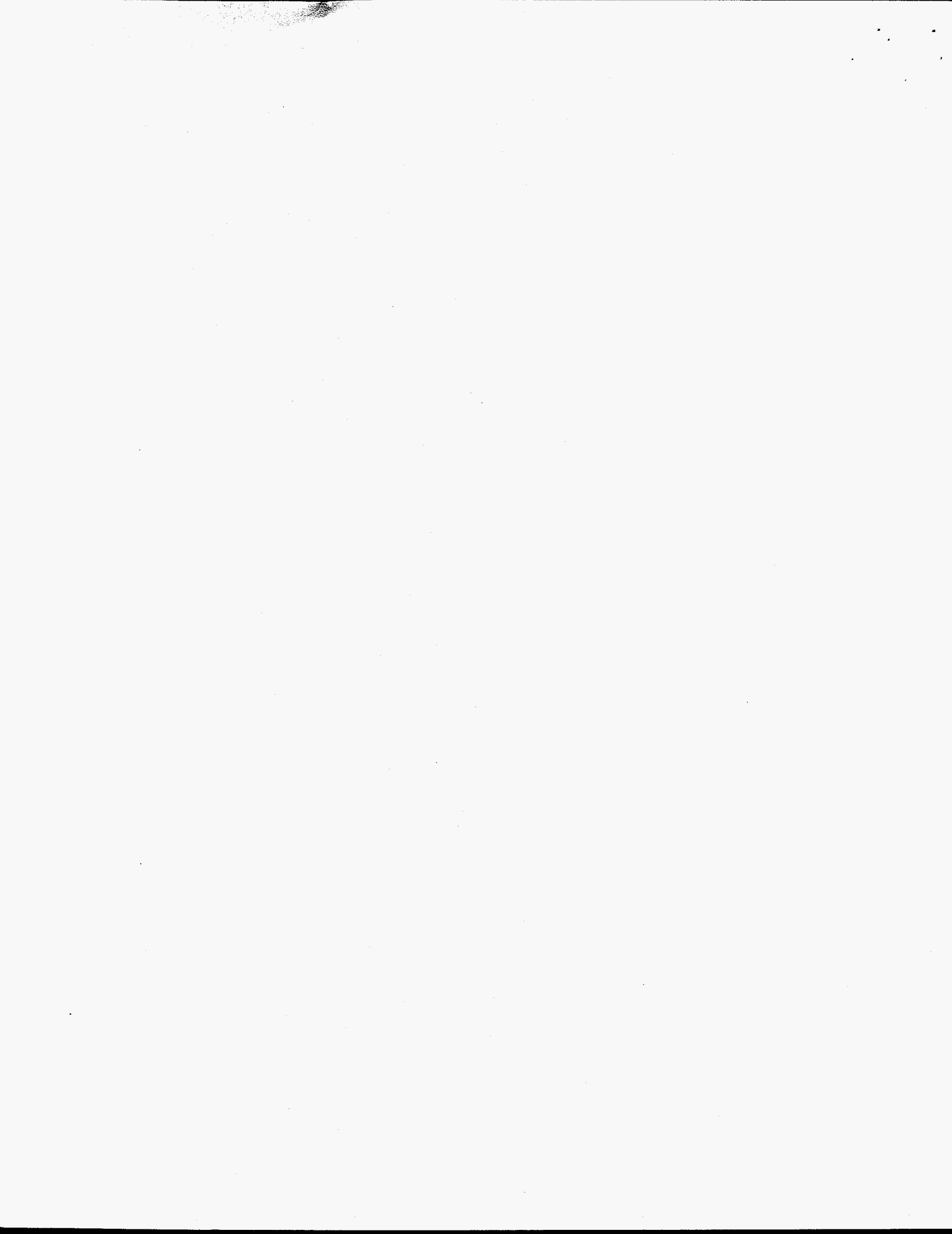
Contents

List of Figures	iii
1 Introduction	1
2 Summary of Improvements to Detonation Modeling Capability	1
3 One-Dimensional Calibration	7
1 The Calibration Test	7
2 PBX9501	9
3 PBXN110	12
4 Parameter Summary	14
4 Two-Dimensional Generator Simulation	14
5 Conclusion	22
6 Acknowledgments	22
References	23
Appendix A Input File for One-Dimensional Calibration Calculations	24
Appendix B Input File for Two-Dimensional Generator Calculations	28



List of Figures

Figure 1	Schematic of magnetocummulative generator and sliding grid technique.	4
Figure 2	Depiction of upstream repositioning rule.	5
Figure 3	Geometry of plate-push calibration problem	8
Figure 4	Copper plate phase space trajectory for PBX9501 calibration. .	10
Figure 5	Data and curve-fit used to calibrate PBX9501 detonation speed.	11
Figure 6	Comparison of PBX9501-driven copper plate trajectory from MACH2 and Los Alamos hydrocode calculations.	12
Figure 7	Data and curve-fit used to calibrate PBX9501 detonation speed.	13
Figure 8	Comparison of PBXN110-driven copper plate trajectory from MACH2 and Los Alamos hydrocode calculations.	13
Figure 9	Numerical grid at $t = 0 \mu s$ for coaxial generator simulation. .	16
Figure 10	Numerical grid at $t = 18 \mu s$ for coaxial generator simulation. .	16
Figure 11	Fluid velocity at $t = 18 \mu s$ for coaxial generator simulation. .	17
Figure 12	Detonated/undetonnated indicator at $t = 18 \mu s$ for coaxial generator simulation.	17
Figure 13	Numerical grid at $t = 40 \mu s$ for coaxial generator simulation. .	18
Figure 14	Fluid velocity at $t = 40 \mu s$ for coaxial generator simulation. .	18
Figure 15	Temperature at $t = 40 \mu s$ for coaxial generator simulation. . .	19
Figure 16	Numerical grid at $t = 60 \mu s$ for coaxial generator simulation. .	20
Figure 17	Fluid velocity at $t = 60 \mu s$ for coaxial generator simulation. .	20
Figure 18	rB_θ contours at $t = 60 \mu s$ for coaxial generator simulation. .	21
Figure 19	Electric current history for 40 cm coaxial generator.	21



1. Introduction

Dramatic improvements have been made to the detonation modeling capability recently incorporated into MACH2. These improvements significantly improve the flexibility of the detonation model, allow for accurate depiction of real explosives, and permit highly efficient modeling of long, coaxial generators. In this document, we will first describe these improvements in some detail. We will then discuss the calibration of the detonation model to two explosive materials, PBX9501 and PBXN110. Finally, we will demonstrate the code's capability for modeling long, coaxial magnetocumulative generators.

2. Summary of Improvements to Detonation Modeling Capability

Several improvements have been made to MACH2 which significantly improve its capability to model explosively driven phenomena. These improvements fall into two categories: those dealing with the manner in which the code treats different materials and different equations-of-state, and those dealing with the manner in which the code manages the numerical grid. The former category, which we will discuss first, is important for all detonation modeling as well as manner other applications, the latter category, discussed second, is important for modeling long, coaxial magnetocumulative generators. But before discussing either of these, we give a brief review of the operation of the detonation model.

A material designated as an explosive will detonate when certain conditions are met. Once these conditions are met, certain operations are performed on the material to simulate the action of detonation and to render the material incapable of detonating again. These conditions and operations are checked and applied on a cell-by-cell basis in each cell which contains material designated as an undetonated explosive. Undetonated explosive is distinguished from detonated explosive on the basis of the value of the variable `con2`. `con2 = 0` denotes undetonated explosive, `con2 = 1` denotes detonated explosive. Two conditions must be met before detonation is allowed. First, the internal energy in the cell must exceed some predetermined threshold value. Second, the artificial viscosity in the cell must be decreasing over time. Simultaneous satisfaction of both conditions ensures that detonation will occur only in response to the zenith of a strong shock. Once these conditions are met, two operations are performed. First, the variable `con2` is changed from its previous value of zero to the new value of one. Second, the internal energy of the cell is incremented by a set, predetermined value. The characteristic of the detonation is most strongly affected by this parameter. Increasing the explosive energy release makes the detonation more intense, and causes it to proceed at a greater rate. The detonation behavior is much less sensitive to the threshold internal energy so long as the value of that parameter is more than a percent or so greater than the

ambient internal energy and less than the sum of the ambient internal energy and the explosive energy release.

The first category of improvements involves the treatment of material identities and the use of different equations-of-state. In our previous work on developing a detonation modeling capability [1], the manner in which different materials and different equations-of-state were handled was somewhat cumbersome. The principal difficulty was the tight coupling between material identity and block identity. Recall that MACH2 is a multiblock code, with logically rectangular sets of cells grouped into individual blocks. Previously, the material identity was synonymous with the block identity. There was one provision which allowed the identity of material in a block to be changed on a cell-by-cell basis, but this could be in operation in one and only one block. It was this provision which was co-opted for use in the detonation model. This restrictive treatment has now been improved significantly.

The new treatment of different materials differs from the old primarily in that the coupling between block identity and material identity has been broken. Material identity is now on a strictly cell-by-cell basis. The one exception is in the initiation phase, where material identity is made on a blockwise basis, but this is largely a matter of convenience. The coupling between equation of state and designation of a material as an explosive has also been broken. Previously, the undetonated explosive was required to be governed by the Gruneisen equation of state, and the detonated explosive was required to be governed by the ideal gas equation of state. While this happens still to be the choice made now, it is a choice, not a requirement. Any material, whether governed by the ideal gas, Gruneisen, or Sesame tabular equation of state, can be designated as an explosive. Similarly, the spent explosive can be governed by any of these equations of state, as well.

Another improvement is in our application of the Gruneisen equation of state. We have analyzed the properties of the equation of state more thoroughly than in our previous efforts. The Gruneisen equation of state can be quite useful in that it allows for negative as well as positive pressure. This allows for the modeling of solid bodies in that by properly initializing the pressure to zero, the solid body will not expand under its own pressure as would happen under the ideal gas equation of state. The Gruneisen pressure consists of two components: the cold pressure, and the thermal component. The former is a function of density, the latter of density and temperature both. The Gruneisen pressure is

$$p = \frac{\rho T(1 + n_f)}{fA} + \frac{\rho c_{so}^2 \left(1 - \frac{\rho_o}{\rho}\right)}{\left[1 - \frac{1}{2}(\gamma_o + 1)\left(1 - \frac{\rho_o}{\rho}\right)\right]} \left\{ \frac{1}{2}(\gamma_1 - 1)\left(1 - \frac{\rho_o}{\rho}\right) + \frac{\rho_o}{\rho} \left[1 - \frac{1}{2}(\gamma_o - 1)\left(1 - \frac{\rho_o}{\rho}\right)\right] \right\} \quad (1)$$

where A is the species atomic weight, and n_f is the number of free electrons per atom. ρ and T are the mass density and temperature of the material, respectively. c_{s0} is referred to as the reference sound speed, and ρ_0 is reference density, which is that density which at absolute zero results in zero pressure. To make use of the zero-pressure property to model a static, solid material, one would like to determine what reference density is required to satisfy $p = 0$ at finite temperature. The resulting equation is cubic in ρ_0 , and in principle can be solved analytically, but it is much more practical so solve the resulting equation numerically. We have written a simple Newton-Raphson root finder to do so, so that for given values for temperature, density, c_{s0} , γ_0 , and γ_1 , the value of the reference density ρ_0 required for vanishing pressure can be calculated to an accuracy of better than one part in a million in just a dozen or so iterations.

The initiation of detonations has been improved to be more flexible. Any material which is designated as an explosive may be initiated in three different ways. One may choose to initiate in a single cell, a row of cells, or a column of cells. The initiation can be made to occur at any time. The choices of time and place of initiation can be different for each material designated as an explosive. The manner in which these choices are communicated to the code is through the variables `detloci(imat)`, `detlocj(imat)`, and `dettim(imat)`, which are read in through the namelist `matmdl`. The variable `imat` is the material identifier. If one wishes to initiate in a single cell, one sets the values of `detloci(imat)` and `detlocj(imat)` to the grid indices i and j , respectively, which identify the desired cell. If one wishes to initiate a column of cells, *i.e.*, in a set of cells with the same grid index i , then one sets `detlocj(imat)` to -1 and `detloci(imat)` to the desired value of i . Similarly, if one wishes to initiate a row of cells, *i.e.*, in a set of cells with the same grid index j , then one sets `detloci(imat)` to -1 and `detlocj(imat)` to the desired value of j . If no value is specified for `dettim(imat)`, then initiation begins at time $t = 0$. To obtain initiation at any other time, one sets the value of `dettim(imat)` to the desired time.

The second category of improvements deals with a new grid management technique, which we call sliding grid. The idea behind this technique is that in the coaxial geometry of the magnetocummulative generator, all of the action takes place in the immediate vicinity of the axially propagating detonation front. The regions upstream and downstream from the axially propagating detonation front can be safely excluded from the active numerical grid. For the downstream region, we expect no disturbances to propagate significantly ahead of the detonation front, and boundary conditions corresponding to the unperturbed materials are appropriate. For the upstream region, we imagine that once the armature has closed to the stator, no more phenomena of physical relevance occur. Thus, as depicted in Figure 1, a region of active grid is moved along with the detonation front.

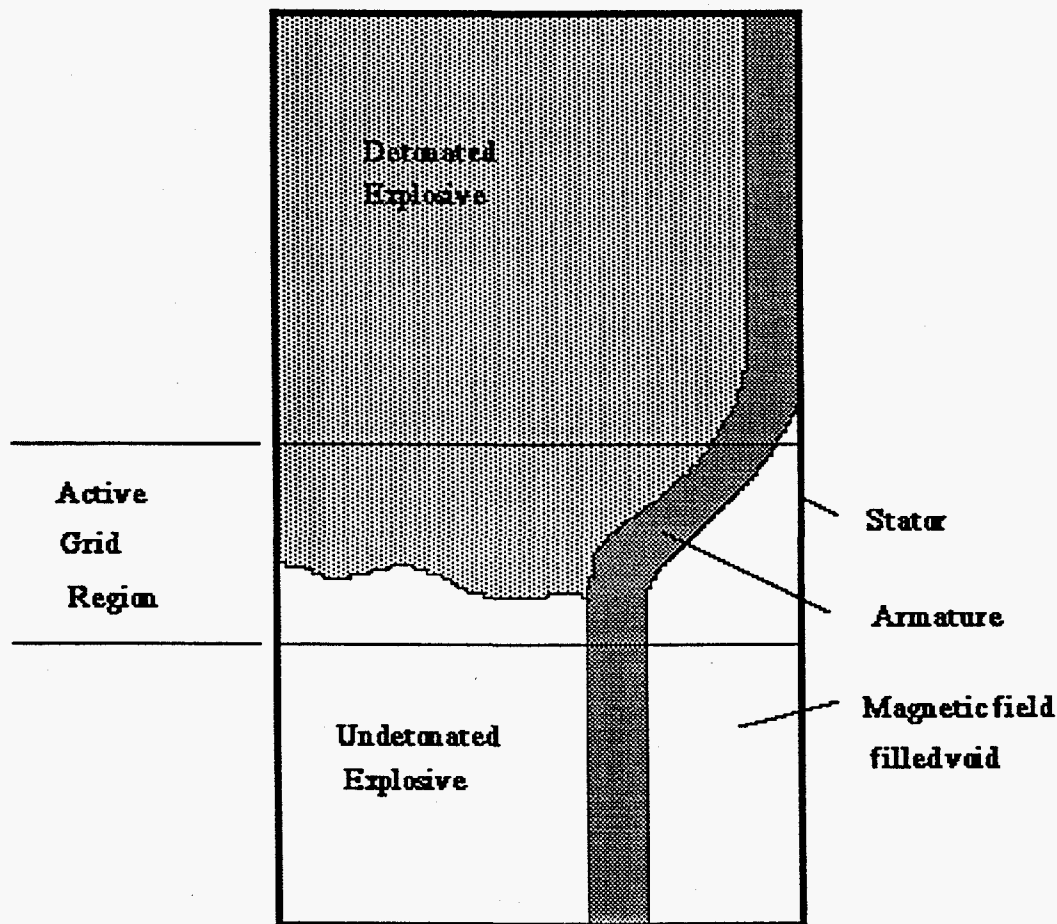


Figure 1 Schematic of magnetocumulative generator and sliding grid technique.

The upstream and downstream boundaries of the grid are constrained to be planes. These planes each are moved according to their own rule. The downstream plane is moved at a constant speed. The user must choose this speed to match the detonation speed, otherwise the detonation front can leave the active grid region. Inflow boundary conditions reflecting the unperturbed, predetonation states of the explosive, armature, and void are applied at the downstream plane.

The upstream plane is moved according to a slightly more complicated rule which Figure 2 helps to illustrate. The repositioning rule is designed so that the armature/stator collision is avoided by keeping the upstream plane just ahead of that collision point. This is accomplished by capturing the outer edge of the armature when it closes to within a certain, pre-set distance of the stator. The grid point, or vertex, which defines the intersection between the upstream plane and the outer edge of the armature plays the principal role in this process. Once this vertex has come to within the minimum distance of the stator, the upstream plane is moved forward a certain distance, Z . As shown in Figure 2, Z is found by projecting from

the current upstream plane a perpendicular ray which emanates from the point defining the minimum armature/stator distance. The intersection between this ray and the line segment joining the first two vertices which define the outer edge of the armature is Z. Each vertex on the old upstream plane is moved forward to the new upstream plane along the line segment which joins it to its first downstream vertex neighbor. This helps to preserve the radial spacing between vertex points on the upstream plane.

The sliding grid technique causes the details of the collision between the armature and stator to be discarded in favor of boundary conditions. The hydrodynamic boundary condition applied at this upstream plane is the continuative boundary condition, *i.e.* the values of the variables in the row of cells immediately adjacent to the upstream plane are simply copied into the ghost cells on the exterior side of that plane.

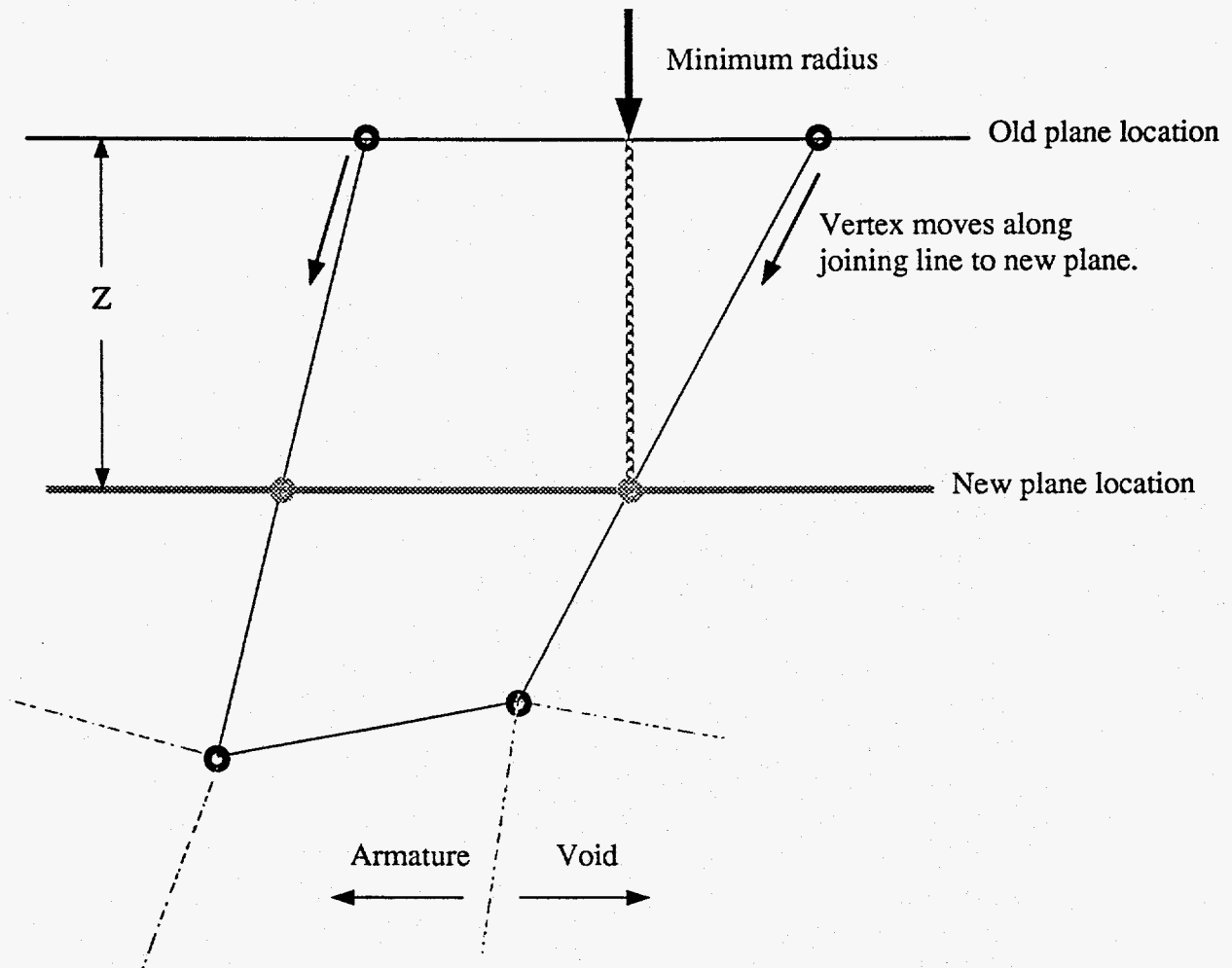


Figure 2 Depiction of upstream repositioning rule.

The benefit of the sliding grid technique is that coaxial generators of arbitrary length can be modeled with a high degree of efficiency. Previously, the entire length of the generator had to be included in the simulation grid. For very long generators, this required using a large number of cells. Of course, the number of cells can be minimized by using cells which are long in the axial direction, but two factors reduce the degree to which this helps. The first is the requirement that the region of the detonation front be adequately resolved. This includes adequately resolving the region in which the armature is undergoing deformation, as well. The mesh generator can be directed to concentrate cells in the axial direction in the vicinity of the detonation front, allowing longer cells can be used away from the front. But the second factor places a limit on how long these cells can be. The numerical algorithms in the code tend to exhibit instability when the aspect ratio of cells exceeds some critical value. Nominally, an aspect ratio of five is the largest one can use with confidence. Thus, even when all the most advanced adaptive gridding features of the code are applied, modeling generators with lengths on the order of meters still requires that a large number of cells be used.

A rough estimate for the minimum number of cells can be made as follows. Consider a coaxial generator with outer radius of 15 cm. Suppose that adequate radial resolution is obtained using 20 cells. This gives an average radial cell dimension of 0.75 cm. The region in which the armature undergoes deformation is roughly 10 cm in axial extent. Suppose a bare minimum of ten cells in the axial direction is adequate to axially resolve this region. This leaves, for a generator with total length of 2 m, 190 cm to resolve axially. With 20 cells distributed over the 15 cm radial dimension, and with a limit on the aspect ratio of 5, this implies a maximum axial cell length of 3.75 cm. This is too large, however, because by directing the mesh generator to concentrate cells into the detonation front region, cells away from this region will be elongated over their initial length. Thus, an initial aspect ratio of say 4 should be used so that once the axial mesh concentration takes place, the resulting maximum aspect ratio will be the target value of 5. This gives a maximum cell length of 3 cm. Thus, the 190 cm not in the detonation front region requires 63 cells in the axial direction. This is still an underestimate because the mesh generator does not support abrupt transitions in cell aspect ratio. Thus, the transition from axially short cells in the detonation front region to longer cells in the less active upstream and downstream regions will cause roughly 50% more cells in the axial direction to be used than estimated so far (using fewer cells will result in cells with aspect ratios larger than desired in the upstream and downstream extremities). Thus, roughly 94 cells in the axial direction are need to resolve the 190 cm away from the detonation front. This brings the total number of cells to $(94 + 10) \times 20 = 2080$ cells. While MACH2 can certainly run a simulation with this number of cells without exorbitant requirements on CPU time, a means of reducing this number of cells by, say a factor of five would allow five times as many simulations to be run for the same cost. This

was the motivation for developing the sliding grid technique.

Finally, the sliding grid technique requires that the circuit model be applied in a specific manner. Initially, the generator contains a certain amount of electrical inductance. If only a fraction of the generator's length is included in the initial grid, then some provision must be made to include in the circuit model that part of the generator inductance corresponding to the portion of the generator not included in the initial grid. As the grid slides, the code will automatically reduce the inductance in accordance to the motion of the grid. For example, suppose that the initial grid has an axial extent of 20 cm, the generator has a total length of 200 cm, and the radial geometry produces an inductance of 1 nH/cm. 180 cm of the generator are not included in the initial grid, so that 180 nH must be included explicitly in the circuit model. This is in addition to any inductance which is exterior to the coaxial portion of the generator.

3. One-Dimensional Calibration

A useful correspondence between simulation and experiment requires that the simulation be capable of reproducing two principal experimental observables: the detonation rate and the detonation pressure. The first governs how rapidly the detonation wave progresses through the explosive material, the second governs the strength of the detonation. A number of standard experiments have been devised over the years which allow these quantities to be inferred from the action of the explosive. One such experiment was chosen for purposes of calibrating the detonation model developed for MACH2. We will first describe that test, then describe the calibration of the detonation model to two different materials: PBX9501 and PBXN110.

3.1 The Calibration Test

Rather than comparing directly to experimental results, our calibration efforts have involved comparing MACH2 results to results from a Los Alamos hydrocode. This code uses a programmed burn detonation model which allows the experimentally determined propagation speed of the detonation wave and the explosive energy release to be input *a priori*.

The calibration problem chosen for this work is a one-dimensional plate-push problem. A one-quarter inch thick copper plate is pushed into a void region by the detonation of two inches of explosive material. The detonation is initiated on the plane farthest from the copper plate, as indicated in Figure 3. The explosive is untamped, that is, an open boundary condition is applied at the initiation plane.

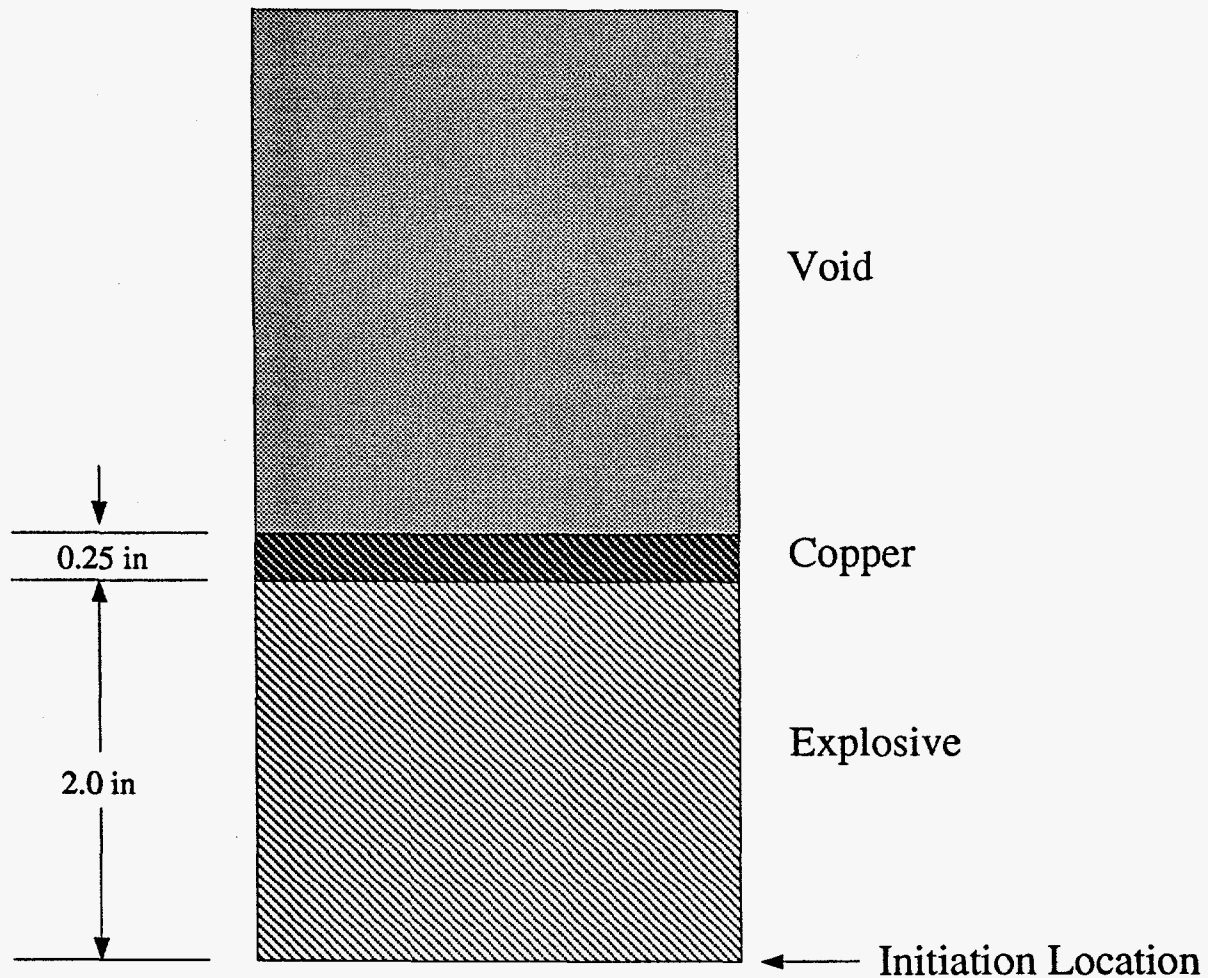


Figure 3 Geometry of plate-push calibration problem

The MACH2 calculations used twenty cells to represent the explosive, four cells to represent the copper plate, and ten cells to represent the void. The Gruneisen equation of state was used for the undetonated explosive, the ideal gas equation of state was used for the spent explosive, and the Sesame tables were used for the equation of state of the copper. The parameters for the Gruneisen equation of state were chosen to ensure that at room temperature, the pressure of that material would be zero. This ensures no expansion or contraction in the absence of any other forces.

Our goal was to match the speed of the detonation wave and to match the speed to which the copper plate was accelerated. The action of the explosive on the copper plate is to provide an accelerating force which is initially quite high, but decreases in time. This decrease has two causes. First, the movement of the copper plate increases the volume available to the spent explosive. Second, and more importantly, the untamped boundary condition gives rise to a rarefaction wave which chases the plate and relieves the pressure. The history of the pressure accelerating the plate

depends sensitively on the equation of state used for the spent explosive, particularly on the sound speed, and on the relation between internal energy and pressure. While we have been able to match the speed of the copper plate, we have not matched the details of the plate's trajectory in phase space. The Los Alamos hydrocode predicts a much flatter phase space trajectory than that observed in the MACH2 runs. The Los Alamos code predicts a quick acceleration followed by a period of very gradually increasing speed. In contrast, MACH2 predicts a much more gradual acceleration. This indicates that the equation of state used for the spent explosive in the Los Alamos hydrocode gave a higher pressure and a higher sound speed than that given by the ideal gas equation of state used for the spent explosive in the MACH2 calculations.

In order to match the speed of the detonation wave, we varied the reference sound speed in the Gruneisen equation of state for the undetonated explosive. To maintain zero pressure in the undetonated explosive, the variation in reference sound speed was accompanied by a variation in the reference density. The speed of the copper plate was varied by adjusting the parameter γ in the ideal gas equation of state:

$$p = (\gamma - 1)\rho\varepsilon \quad (2)$$

where p is the pressure, ρ is the mass density, and ε is the internal energy.

3.2 PBX9501

The relevant defining characteristics of PBX9501 are a density of $1.833 \times 10^3 \text{ kg/m}^3$, an explosive energy release of $5.543 \times 10^6 \text{ J/kg}$, and a planar detonation speed of $0.88 \text{ cm}/\mu\text{s}$. Figure 4 shows the variation in the copper plate phase space trajectory with the γ of the spent explosive's ideal gas equation of state. The variation of plate speed with this parameter is slightly sublinear. If it were not for the dependence of the sound speed on γ , the dependence would be linear.

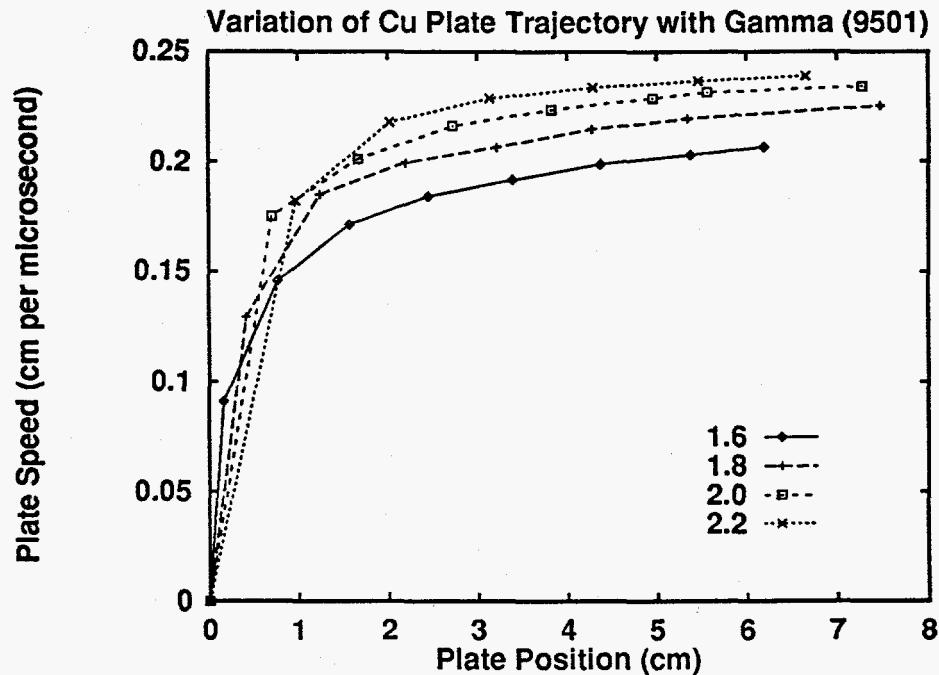


Figure 4 Copper plate phase space trajectory for PBX9501 calibration.

Figure 5 shows the variation in the time required for the two-inch thickness of explosive to detonate with the reference sound speed of the undetonated explosive. Changes in this parameter have only a very small effect on the copper plate phase space trajectory. The data taken from MACH2 calculations are shown as points; the line is an approximate fit to these data. With a detonation speed of $0.88 \text{ cm}/\mu\text{s}$, the time required for 100% detonation of the two inches of explosive is

$$\frac{(2 \text{ in})(2.54 \text{ cm/in})}{0.88 \text{ cm}/\mu\text{s}} = 5.77 \mu\text{s} \quad (3)$$

From the linear fit to the data, this detonation time corresponds to a reference sound speed of 7770 m/s . Using this value yields a detonation time of $5.68 \mu\text{s}$. Given the fact that the timestep used in these calculations was $0.1 \mu\text{s}$, this represents a very good match to the required detonation time.

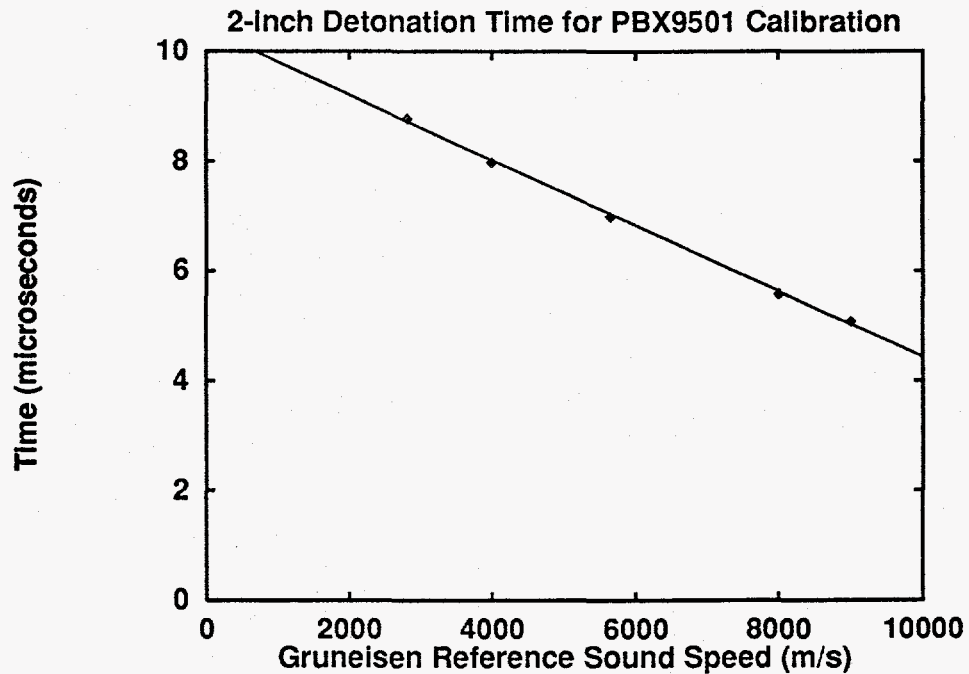


Figure 5 Data and curve-fit used to calibrate PBX9501 detonation speed.

Choosing a value of 2.0 for the γ of the detonated explosive and a value of 7770 m/s for the reference sound speed in the undetonated explosive yields the copper plate phase space trajectory shown in Figure 6. Also shown in this figure is the copper plate trajectory obtained from the Los Alamos hydrocode calculation. The complete set of parameters used for this calculation is tabulated in Section 3.4 below.

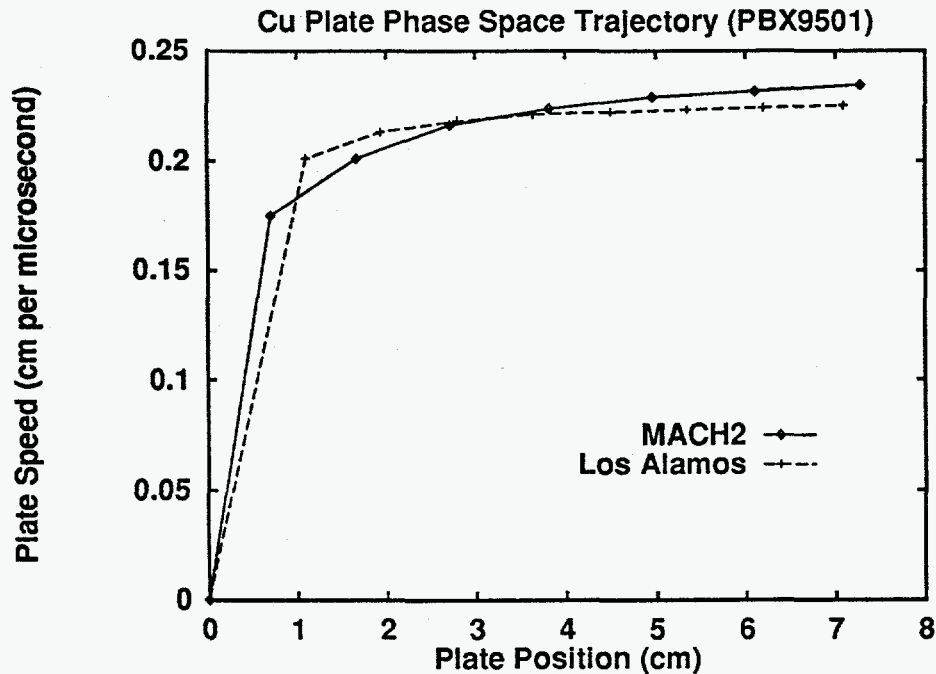


Figure 6 Comparison of PBX9501-driven copper plate trajectory from MACH2 and Los Alamos hydrocode calculations.

3.3 PBXN110

The relevant defining characteristics of PBXN110 are a density of $1.672 \times 10^3 \text{ kg/m}^3$, an explosive energy release of $5.203 \times 10^6 \text{ J/kg}$, and a planar detonation speed of $0.83 \text{ cm}/\mu\text{s}$.

Figure 7 shows the variation in detonation time with the reference sound speed used for the undetonated explosive equation of state. The data obtained from the MACH2 calculations would appear to better fit with a concave function than with a line, but in the neighborhood of the required detonation time of

$$\frac{(2 \text{ in})(2.54 \text{ cm/in})}{0.83 \text{ cm}/\mu\text{s}} = 6.12 \mu\text{s} \quad (4)$$

a linear fit is adequate. A value of 7200 m/s for the reference sound speed gives a detonation time of $6.17 \mu\text{s}$. Figure 8 shows the copper plate phase space trajectory obtained using a value of 1.7 for the γ of the detonated explosive. The plate trajectory obtained from the Los Alamos hydrocode calculation is also shown. Note how, as mentioned previously, the Los Alamos result gives a much flatter trajectory than that calculated by MACH2.

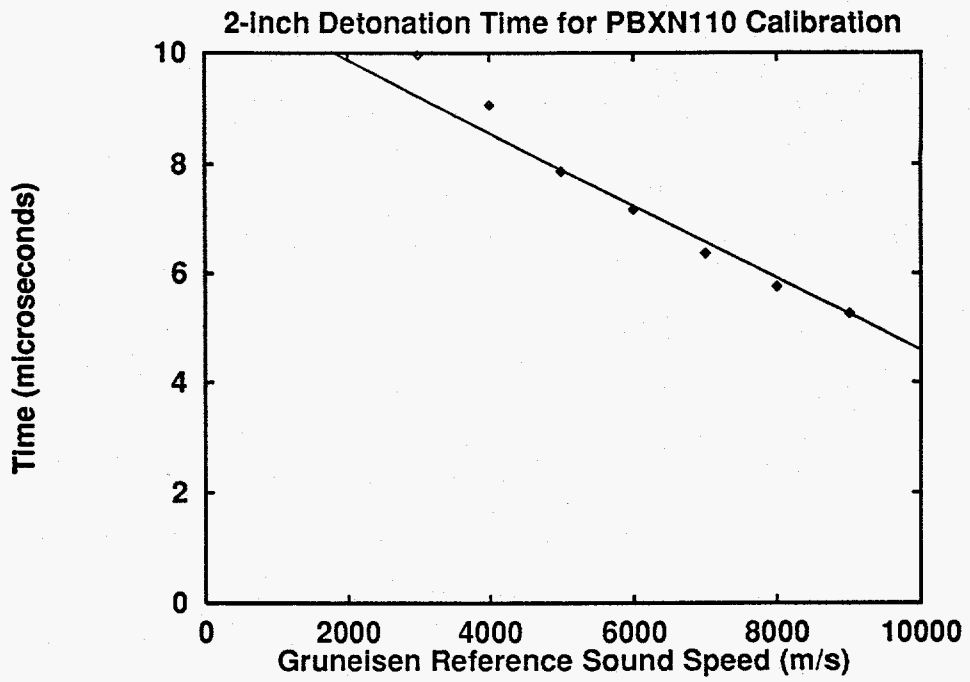


Figure 7 Data and curve-fit used to calibrate PBX9501 detonation speed.

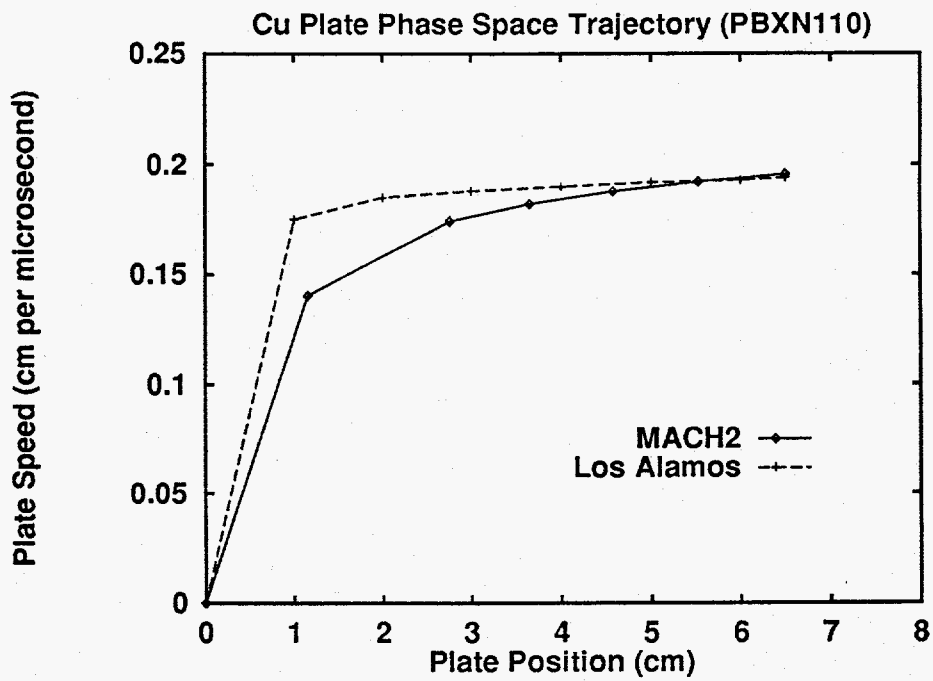


Figure 8 Comparison of PBXN110-driven copper plate trajectory from MACH2 and Los Alamos hydrocode calculations.

3.4 Parameter Summary

Here we list the equation-of-state parameters required to obtain the results above. Appendix A contains a listing of the input file used to drive the one-dimensional calibration calculations. In the input file, the parameters γ_1 , γ_0 , and γ are not input directly. Rather, one inputs these values decreased by unity as indicated in the table. The table indicates the name used in the input file for the corresponding parameter.

Parameter	PBX9501	PBXN110	Variable name
Energy Release (MJ/kg)	5.543	5.203	xplsie
Density (kg/m ³)	1.884×10^3	1.672×10^3	roi
c_{s0}^2 (m ² /s ²)	60.37×10^6	52.0×10^6	csq0
$(\gamma_1 - 1)_{unexploded}$	0.66667	0.66667	gm1 (1)
$(\gamma_0 - 1)_{unexploded}$	1.6	1.6	gm10 (1)
$(\gamma - 1)_{spent}$	1.0	0.7	gm1 (4)

4. Two-Dimensional Generator Simulation

As a demonstration of both the sliding grid technique and of the use of the calibrated explosive model in a two-dimensional setting, we have performed a simulation of a coaxial magnetocumulative generator. The configuration chosen consisted of an aluminum armature of thickness 1 cm with inner radius of 10 cm. The region inside the armature, from the axis to a radius of 10 cm was filled with PBX9501. Exterior to the armature is a void region with radial extent of 4 cm. The total generator length is 40 cm, and the length of the initial grid is 20 cm. Appendix B contains a listing of the input file used to drive this simulation.

The equations of state used in the simulation were for the aluminum armature, Sesame tables, and for PBX9501, the Gruneisen/ideal gas combination precisely as described in the previous section. The void was not a true vacuum, but was filled low

density gas (initial density was $2.7 \times 10^{-2} \text{ kg/m}^3$) governed by the ideal gas equation of state.

The magnetic field filling the void region was generated by a current of 550 kA flowing in the armature. The assumption is that this current has been built up by a driving circuit prior to the start of the simulation, and once the detonation begins, the generator's coupling to this driving circuit is broken. At the downstream end of the generator, we imagine there is a resistor and an inductor in series with the rest of the generator. The value of the resistance was $10^{-5} \Omega$, and for the inductance, 20 nH. The geometry is such that the inductance per unit length of the generator is 61.8 nH/m. With a length of 20 cm of the generator not included in the initial grid, 12.36 nH of the total of 20 nH corresponds to the downstream portion of the generator, leaving 7.64 nH for the external portion of the circuit.

The grid is directed to begin sliding at $18 \mu\text{s}$. The downstream grid plane is assigned a speed of $0.88 \text{ cm}/\mu\text{s}$, a speed which matches the detonation speed of PBX9501. The minimum distance allowed between armature and stator is 1 cm.

Figure 9 shows the initial grid. The cylindrical centerline is located at the left-hand side of the grid. The detonation is initiated in the row of cells at the top of the grid. The boundary condition there is that appropriate for a wall, *i.e.*, the detonation is tamped. The grid and fluid velocity at $18 \mu\text{s}$ are shown in Figures 10 and 11, respectively. The variable used to distinguish between detonated and undetonated explosive, `con2`, is shown in Figure 12. Note that at this time, the detonation front has moved approximately 17.5 cm. This corresponds to a detonation speed of $0.96 \text{ cm}/\mu\text{s}$, which is significantly greater than the desired detonation speed of $0.88 \text{ cm}/\mu\text{s}$. The reason for the higher speed is that in this simulation, the detonation was tamped. Figures 13, 14, and 15 show the grid, fluid velocity, and temperature at $40 \mu\text{s}$. The temperature and grid plots indicate that the detonation front has moved a distance of 17.5 cm in the $22 \mu\text{s}$ since $t = 18 \mu\text{s}$. This corresponds to a detonation speed of $0.795 \text{ cm}/\mu\text{s}$, which is below the one-d detonation speed. The detonation wave has slowed since $t = 18 \mu\text{s}$ due to the increase in volume into which the detonation products may expand. The velocity and temperature plots show that the gas in the void region is being accelerated and shock heated as the volume it occupies shrinks.

2D MAGNETIZED COAX: PROPERTIES ADJUSTED FOR PBX9501
MON12 V9302.
T = 1.000E-11 CYCLE = 0
CALCULATION MESH
1ST X = 0.00E+00
X INC = 2.00E-02
1ST Y = 0.00E+00
Y INC = 5.00E-02

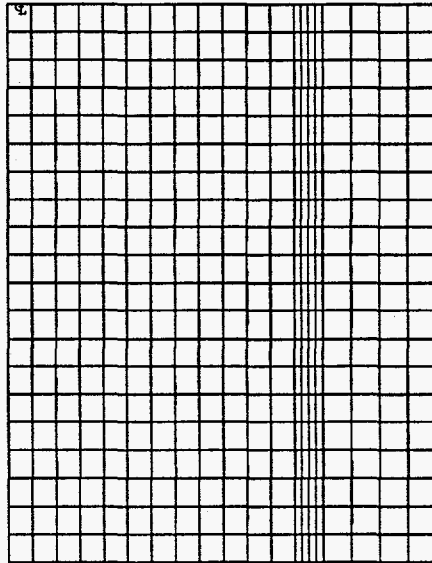


Figure 9 Numerical grid at $t = 0 \mu\text{s}$ for coaxial generator simulation.

2D MAGNETIZED COAX: PROPERTIES ADJUSTED FOR PBX9501
MON12 V9302.
T = 1.800E-05 CYCLE = 194
CALCULATION MESH
1ST X = 0.00E+00
X INC = 2.00E-02
1ST Y = 0.00E+00
Y INC = 5.00E-02

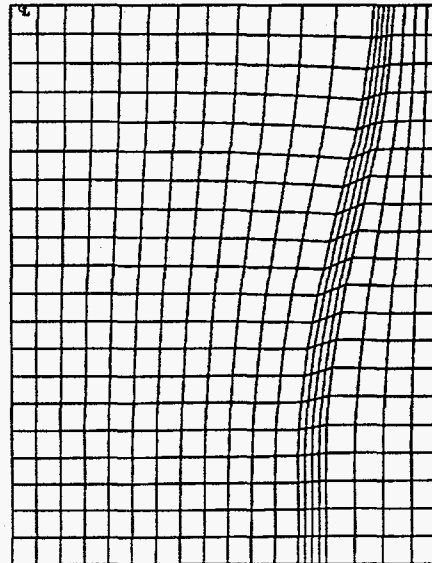


Figure 10 Numerical grid at $t = 18 \mu\text{s}$ for coaxial generator simulation.

2D MAGNETIZED COAX: PROPERTIES ADJUSTED FOR PEX9501
 MON12 V9302.
 T = 1.800E-05 CYCLE = 194
 VELOCITY
 MAX = 2.352E+03

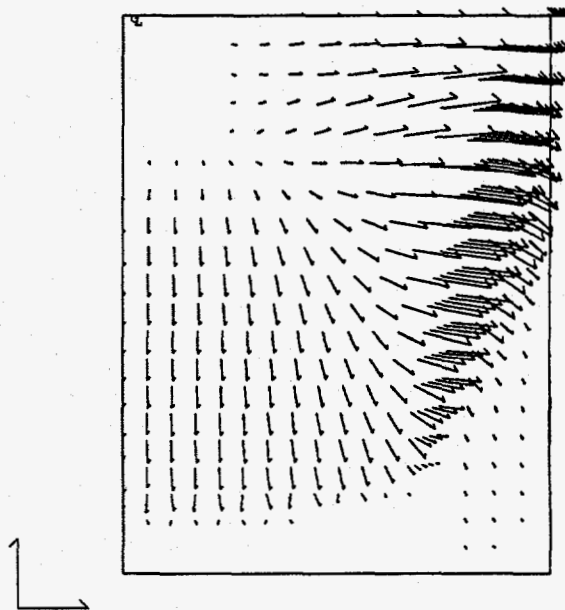


Figure 11 Fluid velocity at $t = 18 \mu\text{s}$ for coaxial generator simulation.

2D MAGNETIZED COAX: PROPERTIES ADJUSTED FOR PEX9501
 MON12 V9302.
 T = 1.800E-05 CYCLE = 194
 CONCENTRATION OF MATERIAL 2
 -- 0.0E+00 B= 2.0E-01 D= 4.0E-01
 F= 6.0E-01 H= 8.0E-01 += 1.0E+00

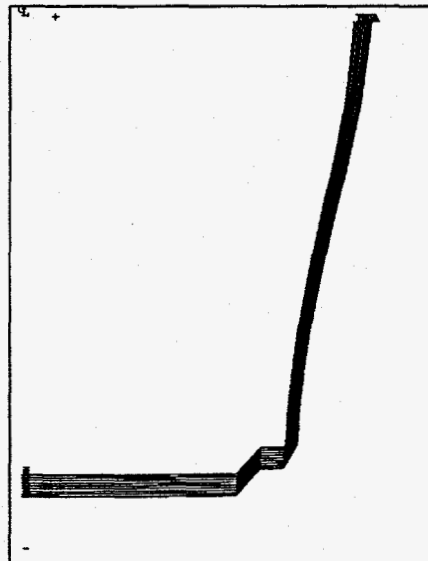


Figure 12 Detonated/undetonnated indicator at $t = 18 \mu\text{s}$ for coaxial generator simulation.

2D MAGNETIZED COAX: PROPERTIES ADJUSTED FOR PBX9501
MON12 V9302.
T = 4.001E-05 CYCLE = 533
CALCULATION MESH
1ST X = 0.00E+00
X INC = 2.00E-02
1ST Y = -1.50E-01
Y INC = 5.00E-02

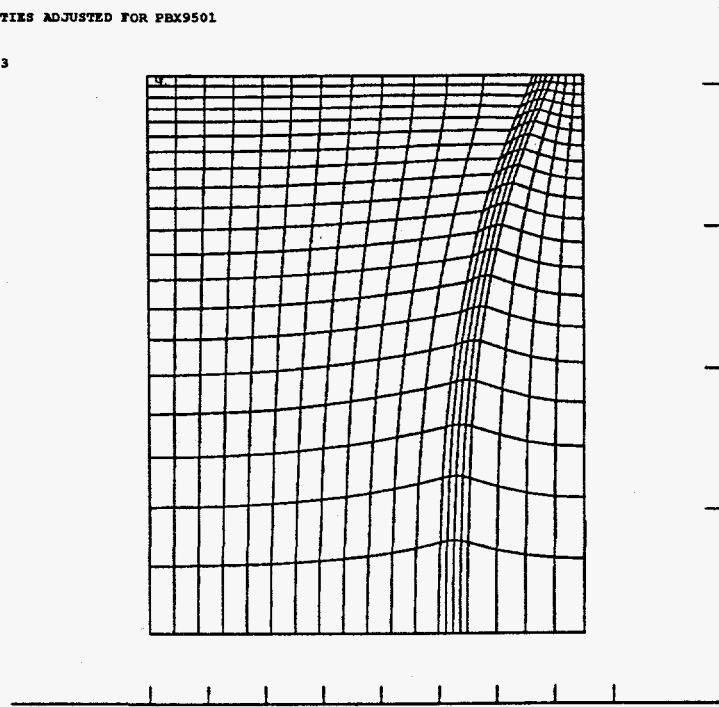


Figure 13 Numerical grid at $t = 40 \mu s$ for coaxial generator simulation.

2D MAGNETIZED COAX: PROPERTIES ADJUSTED FOR PBX9501
MON12 V9302.
T = 4.001E-05 CYCLE = 533
VELOCITY
MAX = 1.311E+04

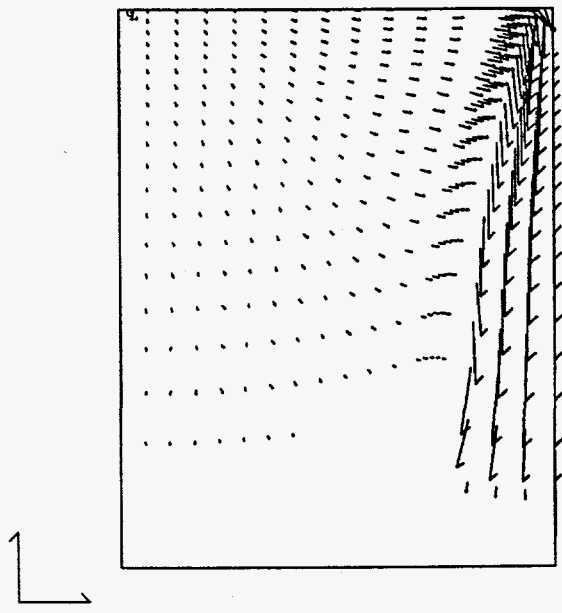


Figure 14 Fluid velocity at $t = 40 \mu s$ for coaxial generator simulation.

2D MAGNETIZED COAX: PROPERTIES ADJUSTED FOR PBX9501
 MCM12 V9302.
 T = 4.001E-05 CYCLE = 533
 TEMPERATURE
 -- 3.5E-03 B= 1.1E-02 D= 3.3E-02
 F= 1.0E-01 H= 3.1E-01 += 9.4E-01



Figure 15 Temperature at $t = 40 \mu s$ for coaxial generator simulation.

The grid and fluid velocity are shown at $60 \mu s$ in Figures 16 and 17, respectively. The detonation of the explosive material was complete at roughly $48 \mu s$. Note that the grid now has an axial extent of just 3 cm. The compression of the gas trapped between the armature and stator has now caused that gas to become warm enough to be mildly conductive. Electrical current is no longer restricted to flow in just armature and stator, but can now flow through the gas in the void region, as shown by the contour plot of rB_θ shown in Figure 18. This represents a current-loss mechanism since the resistivity of the gas is low enough to permit significant current flow, yet it is high enough to allow dissipation of that current. Analysis of the degree of this loss will require more detailed simulation and study.

2D MAGNETIZED COAX: PROPERTIES ADJUSTED FOR PBX9501
MOM12 V9302.
T = 6.000E-05 CYCLE = 1159
CALCULATION MESH
1ST X = 0.00E+00
X INC = 2.00E-02
1ST Y = -1.90E-01
Y INC = 5.00E-03

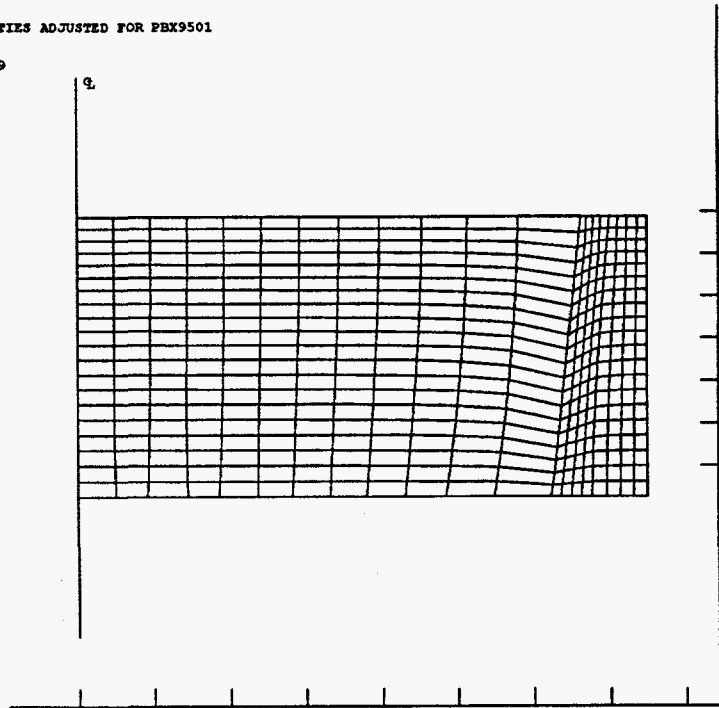


Figure 16 Numerical grid at $t = 60 \mu s$ for coaxial generator simulation.

2D MAGNETIZED COAX: PROPERTIES ADJUSTED FOR PBX9501
MOM12 V9302.
T = 6.000E-05 CYCLE = 1159
VELOCITY
MAX = 2.280E+04

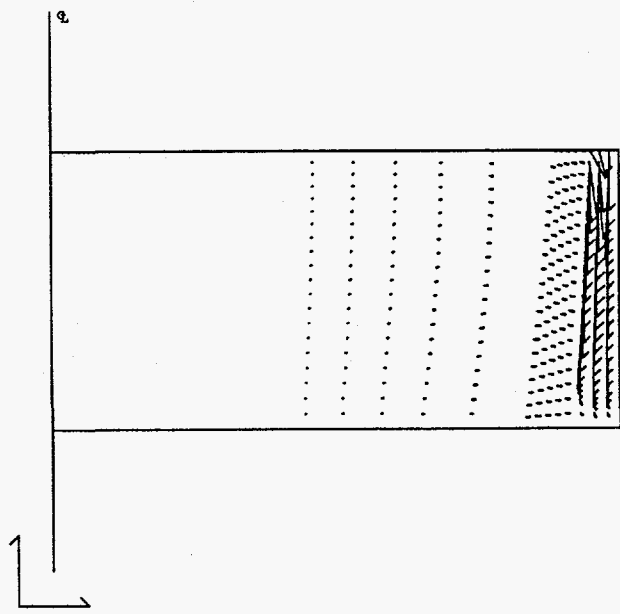


Figure 17 Fluid velocity at $t = 60 \mu s$ for coaxial generator simulation.

2D MAGNETIZED COAX: PROPERTIES ADJUSTED FOR PBX9501
 MON12 V9302.
 T = 6.000E-05 CYCLE = 1159
 RB (AMPS)
 -- 6.4E+00 B= 7.7E+06 D= 1.5E+07
 F= 2.3E+07 H= 3.1E+07 += 3.8E+07

CURRENT(1) = 2.4E+06

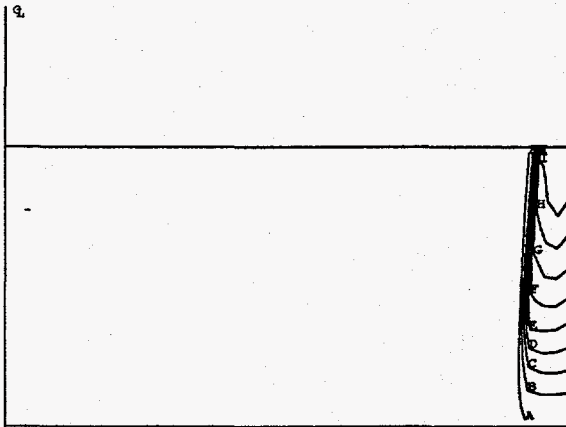


Figure 18 rB_θ contours at $t = 60 \mu s$ for coaxial generator simulation.

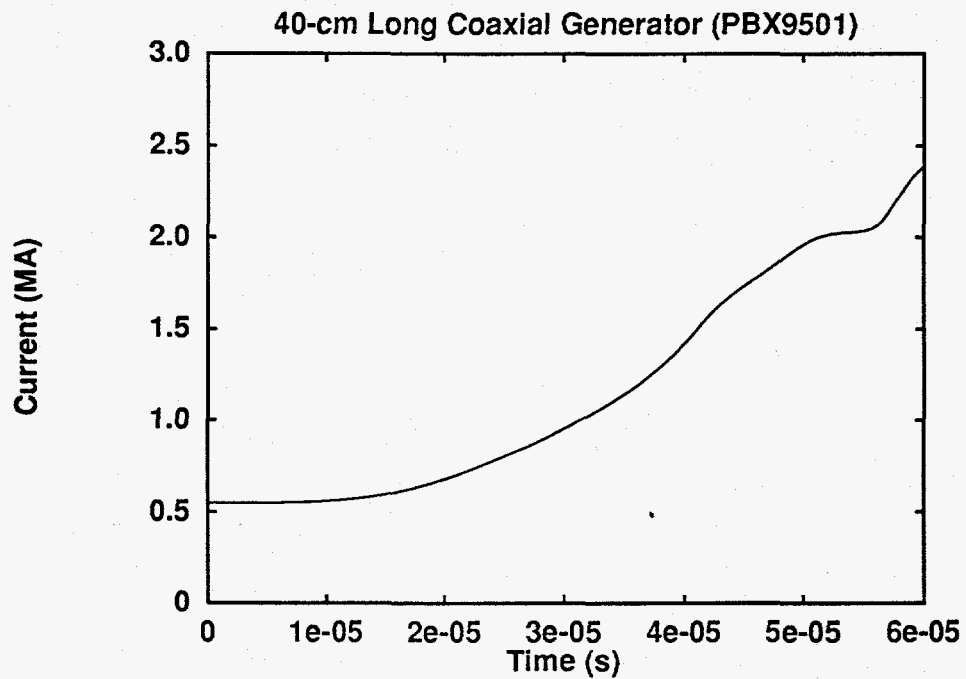


Figure 19 Electric current history for 40 cm coaxial generator.

The current generated is shown in Figure 19. Neglecting resistive dissipation of magnetic flux and the time-rate of change of inductance, the ratio of final current to initial current ought to equal the ratio of initial inductance to final inductance. Initially, the inductance is

$$L_i = L_{ext} + \frac{\mu_0}{2\pi} l \ln \left(\frac{r_{out}}{r_{in}} \right) = 7.64nH + (200nH/m)(0.4m) \ln \left(\frac{0.15m}{0.11m} \right) = 32.3nH \quad (8)$$

At 60 μs , the inductance can be estimated by assuming that all current flows in the armature and stator:

$$L_f \approx L_{ext} + \frac{\mu_0}{2\pi} l \ln \left(\frac{r_{out}}{r_{in}} \right) = 7.64nH + (200nH/m)(0.03m) \ln \left(\frac{0.15m}{0.137m} \right) = 8.2nH \quad (9)$$

The ratio of initial to final inductance is 3.94. The maximum current achieved is 2.43 MA, which is 4.41 times the initial current of 550 kA. The difference between this ratio and the ratio of inductances is likely due to overestimating the inductance of the final configuration. As can be seen in Figure 18, a substantial amount of current is flowing through the gas trapped between the armature and stator, which violates the assumption used in estimating this inductance.

5. Conclusion

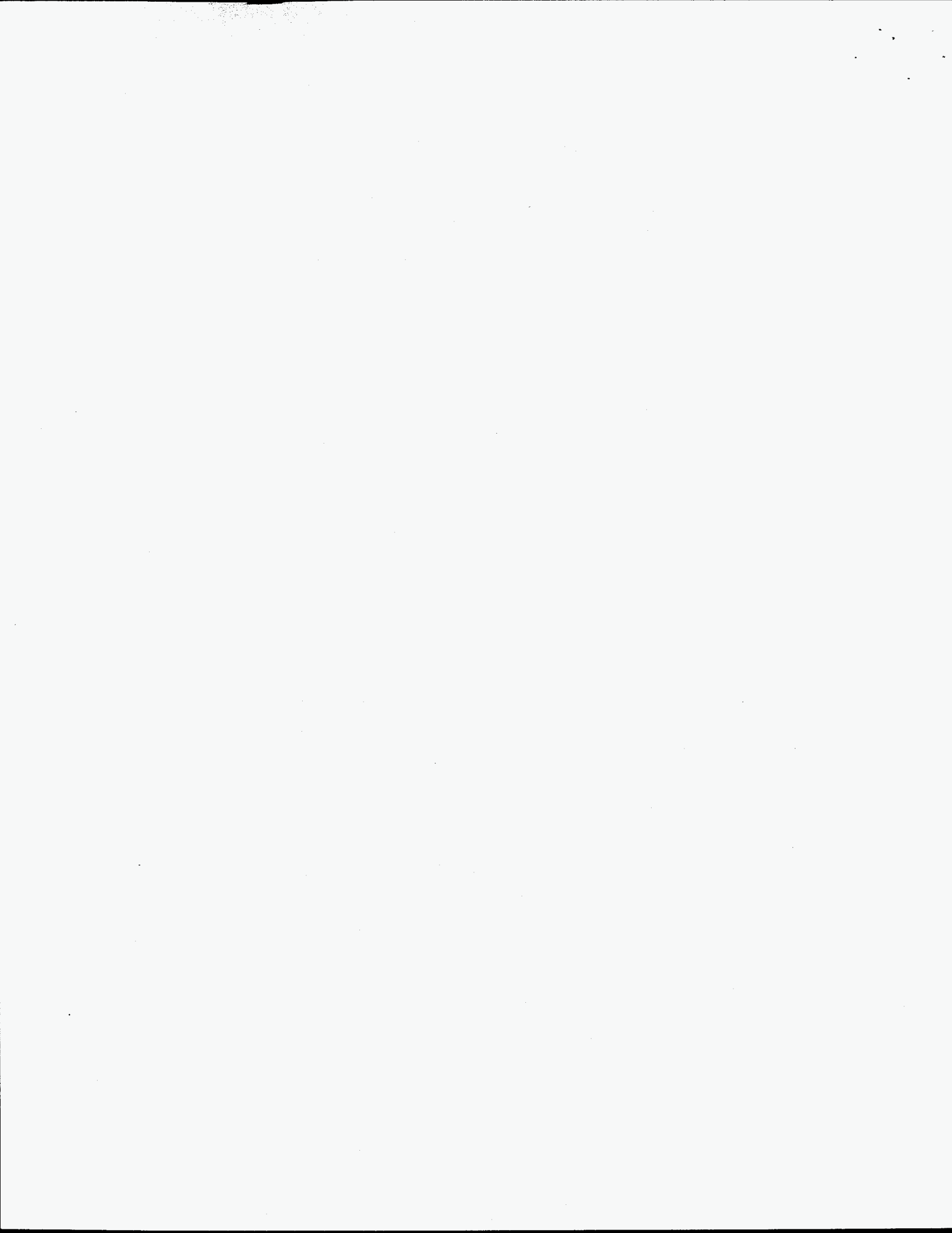
The improvements reported here have significantly improved the detonation modeling capability of MACH2. Any material may be designated as an explosive, and the simulation can contain different explosive materials and different regions of explosive material at the same time. A single cell, a row of cells, or a column of cells may be chosen to initiate the detonation. The detonation may be initiated at any time. With these improvements, parameters corresponding to different explosive materials may be input so that the effect of different detonation characteristics can be assessed. We have determined parameter values which correspond to the explosives PBX9501 and PBXN110. The new grid management technique permits simulation of long coaxial generators without actually having to include the entire length of the generator in the numerical grid. This allows generator simulations to be performed on a much more efficient basis. This new grid management technique is complemented by appropriate modifications to the circuit model. These modifications allow the generator inductance which is not explicitly included in the numerical grid to be included in the circuit in an automatic, self-consistent manner.

6. Acknowledgments

We would like to thank Drs. Bob Reinovsky and Jim Goforth for their continued support for and interest in this work. We would also like to thank Dr. Stan Marsh for his efforts in performing the Los Alamos hydrocode calculations.

References

- [1] J. J. Watrous and M. H. Frese. A dynamic explosive model for MACH2. Technical Report 93-04, NumerEx, 1993.



Appendix A Input File for One-Dimensional Calibration Calculations

CU-PLATE PUSH:

fril5

\$contrl

imns = 150,

twfn = 50.00e-06,

dt = 1.e-9,

dtmax = 1.e-7,

cyl = 0,

eoson = .true.,

explon = .true.,

con2on = .true.,

hydron = .true.,

omegah = 0.66,

volratm = 0.8,

courmax = 1.00,

rmvolrm = 0.2,

mu = 5.6,

radiate = .false.,

fox = 0.1,

cion = .false.,

thmldif = .false.,

flxlmnt = 0.04,

meshon = .true.,

nigen = 0,

niter = 3,

magon = .false.,

! turn off old potential solver

! itpot = 0, for im2oct91991 in dissolv subdirectory

itpot = 20,

potrelx = 0.25,

! magnetic diffusion is on

bdiff = .false.,

! there is no joule heating

jouhtmlt = 0.,

```
multgrd = .true.,
mgmode = 'vcycle' , itmaxrd = 5000,
mglmax = 2,
! sloconv = 0.9,
ncorply = 20,
nvcycmx = 1,
rdrelax = 0.5,
rdtol = 1.e-5,
cntrmin = 1.0,

aresvac = 3.e8,
! aresfdg multiplies the anomolous resistivity
! present value corresponds to ion plasma frequency timescale
aresfdg = 0.e-2,
```

```
$end
$output
```

```
! plots are generated every 100 ns starting at 1000ns; 250ns otherwise
dtp = 1.e-6,
dtrst = 2.e-5,
```

```
intty = 'edits,10',
```

```
contyp(1) = 'log',
plot(5) = 'con2',
plot(6) = 'numvis',
plot(7) = 'sie',
plot(8) = 'momden',
```

```
kcon(1) = 11,
intbound = .false.,
```

```
$end
$ezgeom
```

```
pointx(1) = 0.00e-2,
pointy(1) = 0.00e-2,

pointx(2) = 0.00e-2,
pointy(2) = 5.08e-2,

pointx(3) = 0.00e-2,
pointy(3) = 5.715e-2,

pointx(4) = 0.00e-2,
pointy(4) = 14.00e-2,
```

npnt:


```
pointx(5) = 1.00e-2,  
pointy(5) = 0.00e-2,
```

```
pointx(6) = 1.00e-2,  
pointy(6) = 5.08e-2,
```

```
pointx(7) = 1.00e-2,  
pointy(7) = 5.715e-2,
```

```
pointx(8) = 1.00e-2,  
pointy(8) = 14.0e-2,
```

```
nblk = 3,  
corners(1,1) = 2, 6, 5, 1,  
corners(1,2) = 3, 7, 6, 2,  
corners(1,3) = 4, 8, 7, 3,
```

```
$end  
$sezphys
```

```
icellsg = 2,  
jcellsg = 10,  
roig = 1.894e3,  
tempig = 2.5e-2,  
! sieig = 2.67e05,  
gdvlg = 1.0,
```

```
ang = 5.598417,  
awg = 10.980013,  
densityg = 1.894e03,  
gml0g = 1.57, csq0g = 4.e06,  
tfusig = 1.e-3, hfusig = 1.e02,  
tvapg = 2.e-3, hvapg = 1.e02,  
tdissg = 3.e-3, hdissg = 1.e02,  
tionizeg = 8.e06, hiong = 1.e02,
```

```
$end  
$matmdl
```

```
eosmdl(1) = 'grun', matnam(1) = 'he9501',  
siecrit(1) = 3.5e5, xplsie(1) = 5.543e6,  
density(1) = 1.84004e3,  
explosiv(1) = .true.,  
csq0(1) = 60.37e6,  
gml(1) = 0.6666667,  
gml0(1) = 1.6,  
an(1) = 1.e-3,  
aw(1) = 10.416,
```

```
eosmodl(4) = 'idealgas', matnam(4) = 'spent',  
  gml(4) = 1.,  
  an(4) = 1.e-3,  
  aw(4) = 10.416,  
  density(4) = 1.2e3,  
  csq0(4) = 4.e6,  
  gml0(4) = 0.66667,  
  explosiv(4) = .true.,
```

```
eosmodl(2) = 'tabular', sesanam(2) = 'cu', matnam(2) = 'cu',  
  aw(2) = 63.54, an(2) = 1.e-3, density(2) = 9.14e3,  
eosmodl(3) = 'idealgas', matnam(3) = 'void',
```

```
$end  
$inmesh
```

```
! gruneisen densities are determined so as to give zero pressure  
  roi(1) = 1.833e3, matnami(1) = 'he9501',  
  jcells(1) = 50,  
  detloci(1) = -1, detlocj(1) = 1,  
  hydbc(3,1) = 'flowthru',  
  roflow(3,1) = 1.e-3, tflow(3,1) = 0.025,  
  
  roi(2) = 8.96443e3,  
  jcells(2) = 4, matnami(2) = 'cu',  
  
  roi(3) = 2.7e-2, matnami(3) = 'void',
```

```
$end
```

Appendix B Input File for Two-Dimensional Generator Calculations

2d magnetized coax: properties adjusted for PBX9501
mon12

\$contrl

t = 1.0e-11,
twfn = 70.e-6,
imns = 60,
dt = 1.0e-9,
dtmax = 1.e-7,

hydron = .true.,
 conservh = 0.,
eoson = .true.,

! explon enables the explosive model
explon = .true.,

meshon = .true.,
 nigen = 0,
 niter = 3,

radmodl = "none",
radiate = .false.,
! radsplit = .false.,
! radflxlt = .false.,

thmldif = .false.,
 tdtol = 1.e-4,

bdiff = .true.,
 rdtol = 1.e-4,
 aresfdg = 0.05,

ciron = .true.,

con2on = .true.,
scrctch(1) = 1.e-5,

nsmooth = 4,
wrelax = 0.25,

cyl = 1,

```
volratm = 0.8,  
courmax = 1.0,  
rmvolrm = 0.2,  
itopt = 20,  
mu = 5.6,  
donor = .false.,  
donormn = 1.,  
theb = 1.,  
eps = 1.e-3,  
conserv = 0.,
```

```
mglmax = 1,
```

```
$end  
$output
```

```
ncychist = 1,  
dtrst = 10.0e9,  
dtn = 1000.0e-9,  
dtp = 2.e-6,  
contyp(1) = 'log',  
  plot(8) = 'con2',  
  plot(9) = 'numvis',  
  plot(10) = 'sie',  
  plot(11) = 'momden',
```

```
intty = 'edits,10',
```

```
intbound = .false.,  
kcon(1) = 11,
```

```
$end  
$curnt
```

```
circtype(1) = 'resind',  
  current1(1) = 5.5e5,  
  exres(1) = 1.e-5,  
  exind(1) = 20.e-09,
```

```
$end  
$sezgeom
```

```
npnts = 8,  
pointx(1) = 0.00e-2, pointy(1) = 20.00e-2,  
pointx(2) = 10.00e-2, pointy(2) = 20.00e-2,  
pointx(3) = 10.00e-2, pointy(3) = 0.00e-2,  
pointx(4) = 0.00e-2, pointy(4) = 0.00e-2,  
pointx(5) = 11.00e-2, pointy(5) = 20.00e-2,  
pointx(6) = 11.00e-2, pointy(6) = 0.00e-2,
```

```
pointx(7) = 15.00e-2,pointy(7) = 20.00e-2,  
pointx(8) = 15.00e-2,pointy(8) = 0.00e-2,  
nblk = 3,  
corners(1,1) = 1, 2, 3, 4,  
corners(1,2) = 2, 5, 6, 3,  
corners(1,3) = 5, 7, 8, 6,
```

```
$end  
$ezmats
```

```
rofvacd = 1.e-5,  
rofjould = 1.e-1,  
rofd = 1.e-5,  
rofsiecd = 1.e-5,  
  siecapd = 1.e9,  
  and = 1.,  
  awd = 1.,  
densityd = 1.894e03,  
  gm10d = 2.37, csq0d = 2.e06,  
  tfusid = 1.e-6, hfusid = 1.e-2,  
  tvapd = 2.e-6, hvapd = 1.e-2,  
  tdisssd = 3.e-3, hdisssd = 1.e02,  
  tionized = 8.e06, hiond = 1.e02,
```

```
$end  
$ezphys
```

```
icellsg = 12,  
jcellsg = 20,  
roig = 1.894e3,  
tempig = 2.5e-2,  
gdvlg = 1.0,
```

```
$end  
$matmdl
```

```
numregs = 4,  
eosmodl(1) = 'grun', matnam(1) = 'gel',  
  explosiv(1) = .true.,  
  detloci(1) = -1, detlocj(1) = 20,  
  siecrit(1) = 5.e5, xplsie(1) = 5.543e6,  
  csq0(1) = 60.37e6, gm10(1) = 1.6, density(1) = 1.84004e3,  
  gml(1) = 0.66666667,  
  an(1) = 1.e-3,  
  aw(1) = 10.980013,  
  
eosmodl(4) = 'idealgas', matnam(4) = 'spent', explosiv(4) = .true.,  
  gml(4) = 1.,  
  an(4) = 1.e-3,
```

```

aw(4) = 10.980013,

eosmodl(2) = 'tabular', matnam(2) = 'al-new',
resmodl(2) = 'constant', eta0(2) = 1.e-10,

eosmodl(3) = 'idealgas', matnam(3) = 'gas',

$end
$inmesh

klugbdy = .false.,

! densities are determined so as to give zero pressure
roi(1) = 1.833e3, matnami(1) = 'gel',

roi(2) = 2.7e3, tempi(2) = 0.025,
icells(2) = 4, matnami(2) = 'al-new',
probc(2,2) = 'interfac',

roi(3) = 2.7e-2, matnami(3) = 'gas',
icells(3) = 4,
binit(3) = 'nocurnt',
magzbc(1,3) = 'conductr',
magzbc(3,3) = 'insulatr', currcir(3,3) = 1,
bzi(3) = 1.0, rnomfld = 11.e-2,
bxi(3) = 0., byi(3) = 0.,

gridbc(2,1) = 'smthfix',

gdvl(1) = 1.95,
gdvl(2) = 1.95,
gridbc(2,2) = 'smthfix',
gridbc(4,2) = 'smthfix',

gdvl(3) = 1.95,
gridbc(4,3) = 'smthfix',

$end
$modtim

tmod = 18.e-6,

$end
$inmesh

klugbdy = .true., rstop = 14.e-2,

gdvl(1) = 1.95,
movbdry(3,1) = .true.,

```

```

vbdmov(3,1) = -8.8e3,
gridbc(3,1) = 'fixedgp', gdvlb(3,1) = 0.999999999,
gridbc(2,1) = 'smthfix',

gdvl(2) = 1.95,
gdvlb(3,2) = 1.95,
movbdry(3,2) = .true.,
vbdmov(3,2) = -8.8e3,
gridbc(3,2) = 'fixedgp', gdvlb(3,2) = 0.999999999,
gridbc(2,2) = 'smthfix',
gridbc(4,2) = 'smthfix',

gdvl(3) = 1.95,
movbdry(3,3) = .true.,
vbdmov(3,3) = -8.8e3,
gridbc(3,3) = 'fixedgp', gdvlb(3,3) = 0.999999999,
gridbc(4,3) = 'smthfix',

probc(1,1) = 'contnutv', velbc(1,1) = 'none',
probc(3,1) = 'specfied', velbc(3,1) = 'no slip',
roflow(3,1) = 1.833e3, tflow(3,1) = 0.025,

probc(1,2) = 'contnutv', velbc(1,2) = 'none',
probc(3,2) = 'specfied', velbc(3,2) = 'no slip',
roflow(3,2) = 2.7e3, tflow(3,2) = 0.025,

probc(1,3) = 'wall', velbc(1,3) = 'none',
probc(3,3) = 'specfied', velbc(3,3) = 'no slip',
roflow(3,3) = 2.7e-2, tflow(3,3) = 0.025,

```

```

$end
$modtim

```

```

tmod = 40.e-06,

```

```

$end
$inmesh

```

```

movbdry(3,1) = .false.,
movbdry(3,2) = .false.,
movbdry(3,3) = .false.,

probc(3,1) = 'wall', velbc(3,1) = 'freeslip',
probc(3,2) = 'wall', velbc(3,2) = 'freeslip',
probc(3,3) = 'wall', velbc(3,3) = 'freeslip',

gdvlb(3,1) = 1.0,
gdvlb(3,2) = 1.0,

```

```
gdvl(3) = 0.95,  
gridbc(3,3) = 'normalgl',  
gdvlb(3,3) = 0.95, gdvlc(4,3) = 1.0, gridcc(4,3) = 'fixed',  
gdvlb(4,3) = 1.95,
```

```
$end
```